All-fiber 2–6 μm coherent supercontinuum source based on chalcogenide fibers pumped by an amplified mid-IR soliton laser

B. Kibler, E. Serrano, A. Maldonado, L.-R. Robichaud, S. Duval, M. Bernier, R. Bizot, F. Désévédavy, R. Vallée, Y. Messaddeq, et al.

All-fiber 2-6 µm coherent supercontinuum source based on chalcogenide fibers pumped by an amplified mid-IR soliton laser

B. Kibler[1,*], E. Serrano[1], A. Maldonado[1,2], L-R. Robichaud[3], S. Duval[3], M. Bernier[2], R. Bizot[1], F. Désévédavy[1], R. Vallée[2], Y. Messaddeq[2], and F. Smektala[1]

[1]*Laboratoire Interdisciplinaire Carnot de Bourgogne, UMR 6303 CNRS-Université Bourgogne Franche-Comté, 21078 Dijon, France*

[2]*Centre d'Optique, Photonique et Laser, Université Laval, 2375 rue de la Terrasse, Québec City, QC G1V 0A6, Canada*

[3]*Femtum, 1405 boulevard du Parc technologique, Québec City, QC G1P 4P5, Canada*

[*]*bertrand.kibler@u-bourgogne.fr*

Abstract: We numerically and experimentally investigate an all-fiber configuration of coherent mid-infrared supercontinuum generation in the femtosecond pumping regime. In particular, we demonstrate the advantageous combination of various dispersion-engineered chalcogenide (Ge-Se-Te glass) fibers with a turn-key amplified femtosecond fiber laser delivering 175-fs soliton pulses around 3.4 µm and developed from the erbium-doped fluoride fiber technology. Our results show that compact and coherent octave-spanning fiber supercontinuum sources centered on the 2-5 µm infrared atmospheric window can be obtained with a maximum average power of 50 mW at 25 MHz repetition rate.

Keywords: Nonlinear optics; Mid-infrared supercontinuum generation; Chalcogenide fibers; Solitons

1 Introduction

During the last decade, cascaded fiber systems have emerged as attractive and promising solutions for practical, table-top, and robust mid-infrared (mid-IR) supercontinuum (SC) sources with high spectral power density [1]. Most advanced and recently developed all-fiber-based mid-IR SC

sources are based on the cascade of silica and soft-glass fibers (usually few-meter long segments), enabling a stepwise extension toward the mid-IR starting from an initial near-IR long-pulse laser [2-4]. This implies an optimization procedure for the Raman-induced self-frequency shift of soliton pulses (formed after the initial breakup of the pump pulse) by selecting suitable dispersion-tailored highly nonlinear fiber segments to push forward the SC generation far in the mid-IR. As a result, one can build robust all-fiber systems based on widely available and reliable erbium- and thulium-doped fiber lasers/amplifiers and other passive fiber components from the near-IR technology. Such SC sources that provide enhanced spectroscopy and imaging applications [5-7] have already appeared on sale in some commercial suppliers.

As an alternative or evolution to cascaded fiber systems pumped by near-IR lasers, in the past few years, there has been significant interest in all-fiber SC sources directly pumped by a mid-IR ultrafast fiber laser. It enables investigating broadband SC as well with easier power redistribution into the mid-IR, but more importantly, within the short-pulse (femtosecond) pumping regime in order to better control the temporal coherence properties with engineered dispersion fibers [8-9]. Among the few existing experimental demonstrations that are competitive in terms of spectral bandwidth with most advanced cascaded fiber systems, we can refer to the work by Hudson et al., where a femtosecond mode-locked fiber laser (based on holmium-doped ZBLAN fiber) at 2.9 µm was combined with a chalcogenide tapered fiber [10]. The resulting SC spans from 1.8 to 9.5 µm with over 30 mW of average power at a repetition rate of 42 MHz. More recently, another work by Robichaud et al. reported a record power of 825 mW reached for a 2.5-5µm mid-IR SC based on a standard step-index As_2S_3 fiber pumped by an amplified ultrafast Er^{3+}:ZrF_4 fiber laser providing high peak power femtosecond pulses at 3.6 µm with 58-MHz repetition rate [11].

Now when restricting our analysis to compact fiber SC sources targeting the 3-5µm mid-IR atmospheric window and potential remote sensing applications, it is worth to mention that similar all-fiber SC sources in the femtosecond regime were developed by means of fiber lasers near 2 µm. Salem et al. pumped a step-index indium fluoride fiber resulting in a SC spanning from 1.25 µm to 4.6 µm with a total average power of 250 mW (at 50-MHz repetition rate) and a high degree of coherence across the generated bandwidth [12]. More recently, Kibler et al. reported 1.3-4.3 µm SC bandwidth in a two-zero dispersion step-index tellurite fiber, with 33-mW output power at 19 MHz repetition rate [13].

In this work, we investigate the potential of different dispersion-engineered Ge-Se-Te glass fibers for coherent SC generation within the 2-5µm mid-IR window by means of an amplified ultrafast Er^{3+}:ZrF_4 fiber laser providing high-repetition-rate 175-fs soliton pulses at 3.37 µm. Among several step-index and suspended-core chalcogenide fibers under test, we demonstrate an optimized coherent supercontinuum source spanning from 2 to 6 µm with maximum 50-mW average power at 25-MHz repetition rate. All the experimental results are confirmed by numerical simulations based on the generalized nonlinear Schrödinger equation (GNLSE) for distinct pumping powers. Our all-fiber SC architecture only involves the suitable choice of 4-cm-long segments of chalcogenide fiber to be added to the initial amplified fiber laser based on the erbium-doped fluoride fiber technology. We then expect that such performances will trigger further improvements of such all-fiber coherent mid-IR SC architecture and could lead to practical applications in spectroscopy.

2 Methods

2.1 Pump source and experimental setup used for SC generation

We made use of a simple and compact configuration of SC generation experimental setup, depicted in Fig. 1a, which consists in a commercial, turn-key master oscillator power amplifier based on erbium-doped fluoride fibers (FEMTUM UltraTune 3400) combined with a suitable segment of dispersion-engineered chalcogenide fiber. The seeding source is a 2.8-µm mode-locked femtosecond fiber oscillator at 25-MHz repetition rate [14] that is amplified and redshifted at 3.37 µm through soliton self-frequency shift (SSFS) in a single-pass amplifier stage, as recently demonstrated in Ref. [15]. A long-pass filter (LPF) at 2.9 µm before the coupling lens is used to remove the residual pump after the SSFS process in the amplifier stage. After filtering the fiber amplifier output, we then have two mid-IR shifted solitons generated during the SFSS, namely S1 and S2, for an average power of 280 mW. Figure 1b shows the corresponding spectrum measured. By using a simple fitting procedure, we found that S1 can be accurately modeled by a Fourier-transform sech-pulse with duration at full width half maximum (FWHM) of 175 fs (i.e., 1.8-THz spectral bandwidth). This main soliton (S1) centered at 3.37 µm contains about 90% of the available energy beyond 2.9 µm. The secondary soliton (S2) with remaining energy is located at 3 µm. Next, our study of SC generation was performed with the free-space coupling option (i.e.,

collimated output laser beam) to avoid any damage of output fiber facet during optimization procedures with several chalcogenide fibers. However, note that for more robust SC schemes, suitable splicing methods could be investigated to directly connect the most suitable chalcogenide fiber with the fiber output of the pump source. Before coupling into the chalcogenide fiber, both linear polarization and input power of pump pulses are controlled via the combination of a half-wave plate and an optical density. Fiber coupling was then performed by means of several ZnSe lenses with specific 3-5 μm AR coating and distinct focal lengths (from 4 to 6 mm) as a function of the fiber core diameter. Overall, the free-space optics reduced the total available incident power by ~15%. As a consequence, the available average power of the main mid-IR shifted soliton pump (S1) is now 213 mW, thus corresponding to ~50-kW peak power. Our chalcogenide fibers were cleaved by means of a scalpel blade and quality of the interfaces was carefully checked under microscope before mounting a few-cm long fiber sample onto a 3-axis holder. Pump pulses are then coupled into the fundamental guided mode. Our total coupling efficiency is rather low due to significant Fresnel reflection (nearly 20%), and we obtained a coupling factor about 15-40% in our fibers with core diameters varying from 4 to 13 μm (see Sec. 2.2), so that SC generation can be investigated with a maximum injected (S1) peak power of roughly 15 kW. At the output of our chalcogenide fibers, the SC light generated is directly collected by a 1-m long multimode fluoride (InF_3) fiber with the butt-coupling technique. This multimode fiber (100-μm core) exhibits an excellent transmission over the 0.35-5.5 μm spectral range and allows to characterize the SC spectrum by means an optical spectrum analyzer (Yokogawa, AQ6377) over the 1.9-5.5 μm range. For SC bandwidth beyond 5.5 μm, we collect the SC light by means of ZnSe lens, and next an off-axis parabolic gold mirror sends the mid-IR light into a monochromator combined with a HgCdTe (MCT) cooled detector operating up to 12 μm. For each SC measurement, its corresponding average power was measured by means of a thermal power sensor. Note that we were not able to pump all the chalcogenide fibers with the maximum available pump power due to some damage issues discussed in the following.

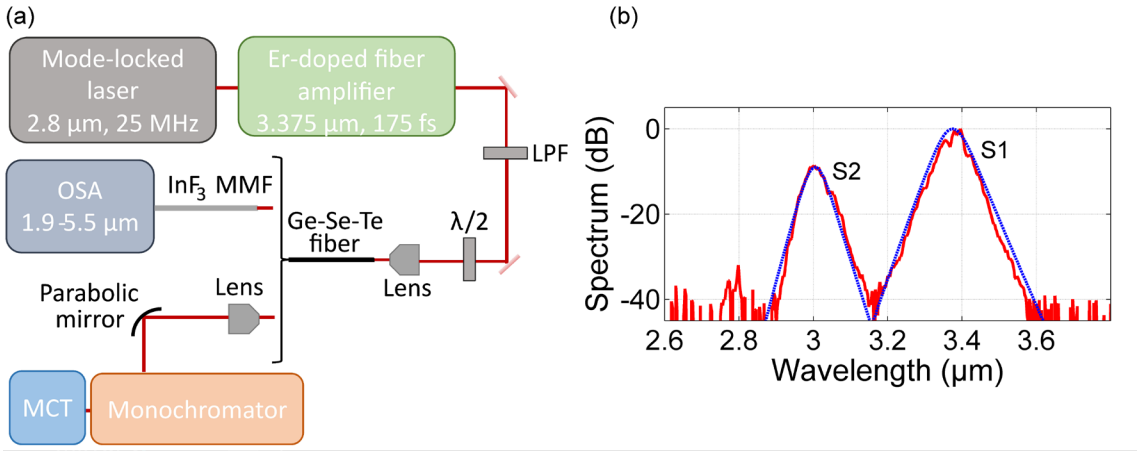

Figure 1. (a) Experimental setup for SC generation in our Ge-Se-Te fibers. LPF: long-pass filter; Att: optical attenuator; λ/2: half-wave plate, MCT: HgCdTe cooled detector. (b) Corresponding measured spectrum (red solid line) of the pulsed pump before injection into the distinct chalcogenide (Ge-Se-Te) fibers under test (i.e., after LPF). S1: first mid-IR shifted-soliton that contains 90% of output average power of the fiber amplifier beyond 2.9 µm. S2: secondary shifted soliton. RP: residual pump after the long-pass filtering. Blue curves correspond to fitting spectra of FT-soliton (sech-) pulses.

2.2 Fabrication and properties of designed chalcogenide fibers

We developed two kinds of chalcogenide fibers based on the Ge-Se-Te ternary glass system for SC generation with the above mid-IR soliton pump, namely step-index fibers (SIF) and suspended-core (microstructured) fibers (SCF). The fabrication of single-material optical fibers (including or without a suspended core) as well as step-index ones based on such a glass free of highly toxic elements such as arsenic and antimony was already described in Refs. [16-17]. Moreover, ultra-broadband SC generation (from 1.7 to 18 µm) was also demonstrated with such fibers with low residual losses pumped by bulky high-power ultrashort laser sources near 8 µm at 1-kHz repetition rate [18], thus confirming its relevance for nonlinear applications in the mid-IR region. We here recall below some of the most important details of fiber fabrication. We selected the Se-rich part of the pseudo-binary $GeSe_4$-$GeTe_4$, known to be compatible with fiber technology, from glass purification through distillation procedure to drawing operations.

For step-index fibers, the cladding and core compositions are $Ge_{20}Se_{70}Te_{10}$ and $Ge_{20}Se_{60}Te_{20}$, respectively. The index difference between the two compositions is about 0.09 over the mid-IR

range [16]. Glass rods are synthesized by the standard melt quenching method. Stoichiometric quantities of high purity elements (5N) are weighted and then inserted into silica ampoules, then evacuated for several hours and heated up to remove superficial oxides as well as free water adsorbed on surface. Next, the precursors are gathered in the same ampoule in which oxygen and hydrogen getters (Al and $TeCl_4$) are added for further purification. The batch is then heated to fusion and further quenched in the glassy state, before to be first distilled under a dynamic vacuum. Volatile impurities are evacuated and trapped. Then, the silica ampoule in which the distilled glass has condensed is sealed and placed in a two-zone furnace for a second static distillation to separate the remaining traces of refractory particles responsible for optical scattering. Finally, the glass batch is inserted into a rocking furnace for the last refining process, next quenched and finally annealed. Step-index preforms were fabricated by means of the rod-in-tube technique, and then drawn into step-index fibers with controllable outer and core diameters. An example of SIF with 10-µm core diameter is shown in Fig. 2a. In the case of suspended core fibers, we made use of a purified $Ge_{20}Se_{70}Te_{10}$ glass rod, and three holes are drilled around the center with 1 mm in diameter and 30 mm in length. During the drawing process, these holes allow the formation of the air-suspended structure with three fine bridges supporting the core. A nitrogen gas pressure enables to control the hole's size, several meters of fiber with distinct suspended-core diameters were obtained (see Fig. 2a that depicts a SCF with 9-µm core diameter).

Figure 2b compares linear losses measured (cutback method) over the 2-7 µm wavelength range for a step-index fiber and a suspended-core fiber with large core diameters in both cases. Typically, our fibers exhibit background losses in the range 1-6 dB/m beyond 3 µm, except at the Se-H related absorption peak near 4.6 µm that remains below 10-15 dB/m. Note that such losses will be negligible on cm-long propagations investigated for SC generation in the following. Next, we performed numerical simulations of fiber modal properties based on the fiber geometry obtained from the scanning electron microscope (SEM) analysis and by means of a commercial software using a beam propagation method (RSoft product). We then found that a variety of dispersive properties can be explored for SC generation at our pumping wavelength $\lambda_0 = 3.37$ µm. Calculated dispersion curves, as a function of wavelength of the fundamental guided mode, for distinct core diameters of SIF and SCF designs are shown in Fig. 2c. Corresponding effective mode areas are reported in Fig. 2d, thus providing information about light confinement and resulting nonlinear coefficient calculated as $\gamma = 2\pi n_2/\lambda_0 A_{eff}$, with nonlinear refractive index $n_2 = 8.3\times10^{-18}$

m^2/W [17]. The simple SIF design (for core diameter between 7 and 13 µm) with moderate index-difference only provides strong normal dispersion ($\beta_2 > 0$) at the pump wavelength, since it is far from the intrinsic zero dispersion wavelength (ZDW) of the bulk glass (located beyond 6.5 µm). The main interest here is that all-normal dispersive regime can be reached with moderate core diameter as well as enhanced confinement. By contrast, the SCF design provides a clear flexibility in the dispersive properties at the pump wavelength. With similar core diameters as for SIF, we can strongly reduce the normal dispersion since the ZDW can be shifted below 4 µm, thanks to the strong index difference. By choosing smaller core diameters below 6 µm, we could also investigate SC generation in the anomalous dispersion regime ($\beta_2 < 0$).

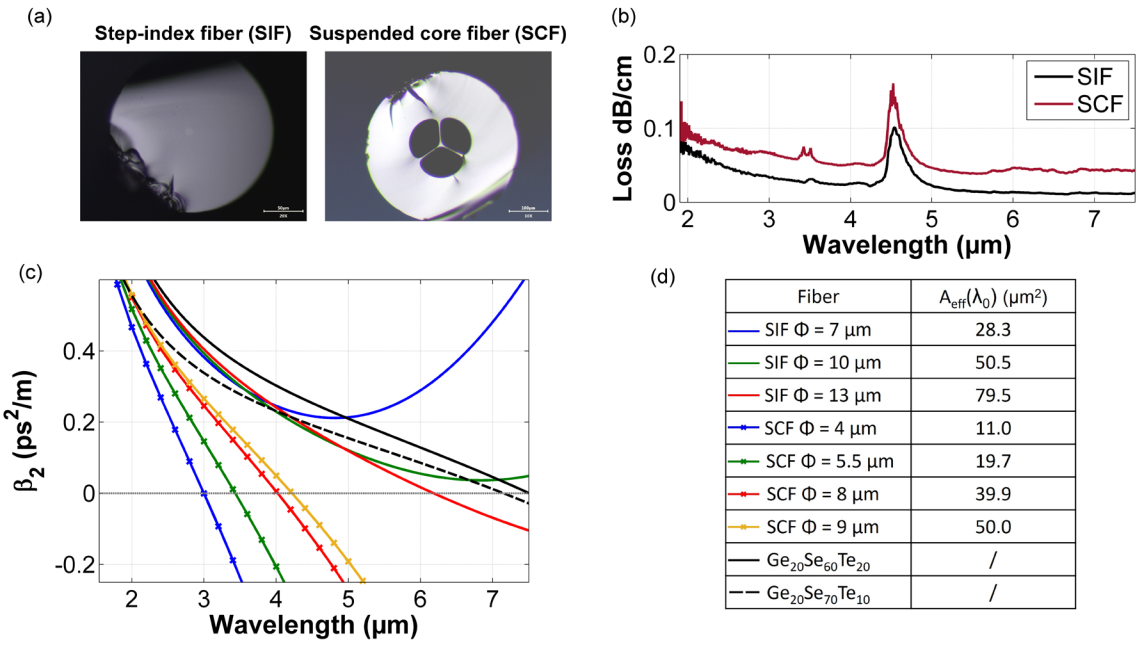

Figure 2. (a) Cross-sections of (left) step-index and (right) suspended-core Ge-Se-Te fibers captured by means of a scanning electron microscope. (b) Measured linear losses for SIF and SCF designs with a large core diameter. (c) Wavelength-dependent curves of group-velocity dispersion β_2 of the fundamental guided mode of SIFs and SCFs with distinct core diameters (values are indicated in the adjacent table). (d) Corresponding effective mode area calculated at the pump wavelength.

2.3 Numerical modeling

In the following, we also report numerical simulations of the nonlinear pulse propagation in our chalcogenide fibers to confirm the SC bandwidth measured with the experimental setup above-described, and accordingly to the pumping laser parameters. Our modelling is based on the commonly-used generalized nonlinear Schrödinger equation that includes the full dispersion curve of the fundamental guided mode of each fiber under test (as shown in Fig. 2), both instantaneous Kerr and delayed Raman nonlinear responses, and the dispersion of nonlinearity including the frequency dependence of the effective mode area [8]. This equation governs the evolution of the complex envelope of the electrical field. For the Raman response function, we used an intermediate-broadening model using convolutions of Lorentzians and Gaussians adapted from spontaneous Raman scattering spectra and estimated Raman gain coefficient given in Ref. [19-20]. The contribution of the delayed Raman response was found to be $f_R = 0.21$. Our simulations also include the fiber losses measured in Fig. 2.

The dependence of SC stability on the input pulse characteristics and the fiber parameters has been extensively studied during the last decade [8,21]. The anomalous dispersion regime is known to favor the competition of coherent (soliton dynamics) and incoherent (modulation instability) spectral broadening mechanisms. It is well-accepted to consider a pump soliton number of $N < 10$ as a general rule to maintain high coherence and pulse-to-pulse stability. Recall that N is defined as follows: $N^2 = L_D / L_{NL} = \gamma P_0 T_0^2 / |\beta_2| =$, where P_0 is the peak power, T_0 is the half-width (at 1/e-intensity point) of the input soliton pulse, and β_2 is the group velocity dispersion at the pump wavelength. $L_D = {T_0}^2 / |\beta_2|$ refers to the dispersion length, and $L_{NL} = 1/\gamma P_0$ to the nonlinear length. On the contrary, all-normal dispersion fibers allow highly coherent SC to be designed for initial N value up to a few hundreds. Then, we analyze the coherence properties associated with the SC spectrum, in a similar way to Ref. [8]. We specifically perform 200 simulations with different random input noise imposed on the input pulse for each fiber. The ensemble of output SC fields allows the calculation of the complex degree of first-order coherence g_{12} defined at each wavelength in the SC, typically used to characterize the shot-to-shot stability of SC sources [8].

3 Results

3.1 SC generation in step-index Ge-Se-Te fibers

We first investigate SC generation in three step-index Ge-Se-Te fibers with the following core diameters 7, 10, and 13 µm. As shown previously in Fig. 2, they almost exhibit the same normal dispersion whereas distinct nonlinear efficiency can be expected. Figure 3 shows both experimental (left panels) and numerical (right panels) results obtained for two different input peak powers. For the lowest input power ($P_0 = 1.8$ kW), we clearly observe that SC generation is enhanced in small-core fibers due to a stronger nonlinear coefficient. When increasing P_0 up to 6.7 kW, we note that the SC bandwidth can cover the 2.5-5 µm wavelength range in the 10-µm core SIF. We were not able to observe SC generation with the same power in the smallest core SIF because of damage on the input fiber facet. Similar issues also arose at higher pump power for all the SIFs. We confirm our SC experiments with numerical simulations taking into account the single main soliton S1 as pump. The agreement is excellent over the full SC spectrum, one can only note few discrepancies such as, a small dip around 4.2-4.3µm in the experimental spectrum (not present in the simulation) due to the common CO_2 absorption in the atmosphere, and a small bump around 3 µm due to the remaining secondary soliton from the pumping source. Pumping in the strong normal dispersion regime implies that SC generation is here driven by self-phase modulation and optical wave-breaking [22], thus the spectrum remains nearly symmetric around the pump wavelength and narrower than in anomalous dispersion regime. Then, the typical features are (i) the good spectral flatness, (ii) the single-pulse preservation and its quasi-linear chirping, and (iii) the stability to input noise, which guarantees a full SC coherence, as reported in Fig. 3 (right panels). To achieve the largest spectrum with high spectral flatness, it is convenient to propagate the input pulse until wave-breaking occurs. By using the empirical L_D/N scaling of wave-breaking distance, a rough estimate of the maximum spectral broadening (-3dB bandwidth) for secant-hyperbolic pulses can be found as 1.7 N [22] (neglecting higher-order dispersions and the self-steepening effect). In our three experimental configurations, β_2 is in the range 0.31 - 0.34 ps^2 m^{-1} and $\gamma =$ 0.54, 0.30, and 0.19 W^{-1} m^{-1}, respectively. We find that all our SC spectra recorded after 4 cm of propagation (whatever the input peak power) are well obtained at maximal spectral broadening even with such moderate soliton numbers ($N < 10$). At $P_0 = 6.7$ kW, the spectral broadening factor in the 10-µm core SIF is expected to be 13 times the initial 1.8-THz spectral width (i.e., 23 THz). Experimentally and

numerically, the corresponding SC spectrum spans from 3 to 3.8 μm at -3dB, which corroborates the above prediction. We also achieved a −20 dB bandwidth from 2.7 to 4.7 μm (i.e., 50 THz) at this 6.7-kW peak power, we could expect larger SC bandwidth at the maximum power available (see section 4).

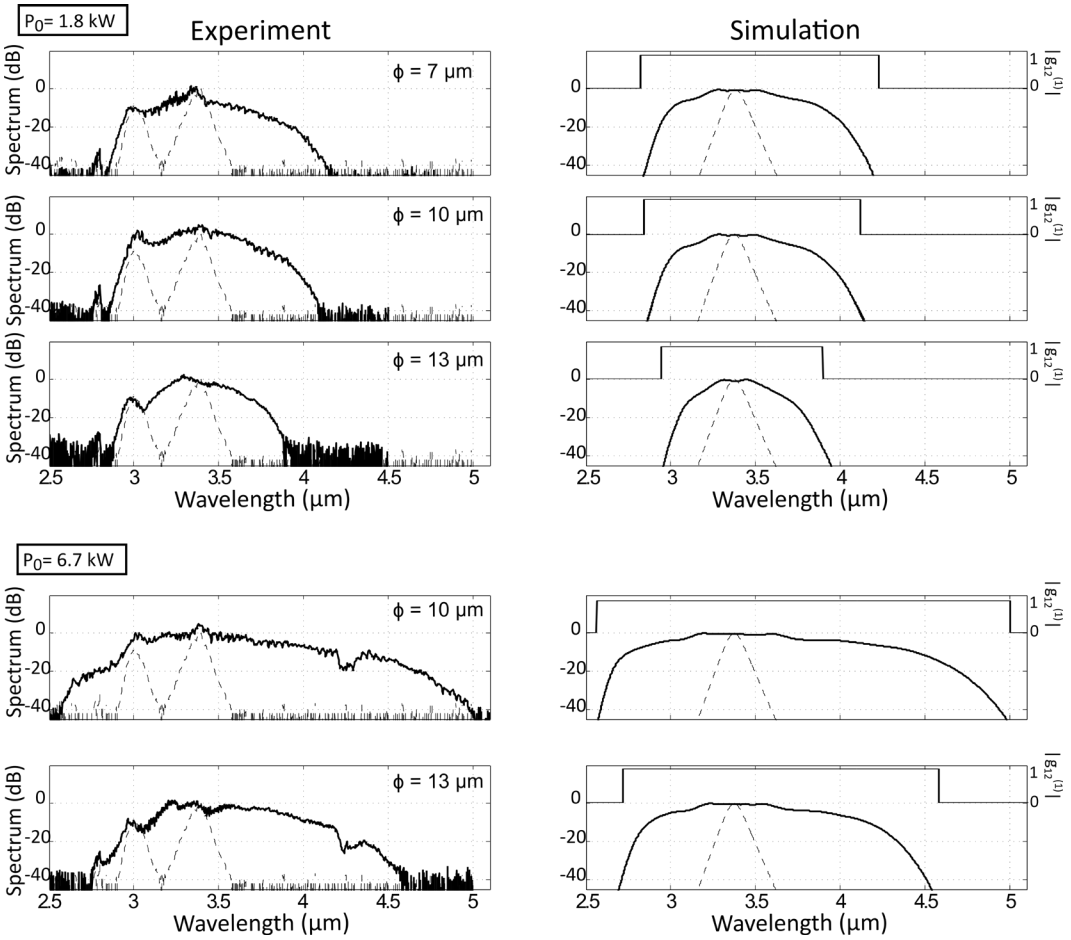

Figure 3. SC spectra obtained in step-index Ge-Se-Te fibers with distinct core diameters (7, 10, and 13 μm) and for two input peak powers (1.8 and 6.7 kW). Left panels: experimental SC measurements. Dashed lines indicate the spectrum of the input pump source. Right panels: corresponding numerical results of SC generation. Left axis provides the average SC spectrum obtained 200 simulations. Dashed lines indicate the input pump spectrum considered. Right axis shows the calculated modulus of the complex degree of first-order coherence (a value of 1 denotes perfect coherence).

3.2 SC generation in Ge-Se-Te fibers with large suspended-core

In a second set of experiments, we investigate SC generation in two suspended-core Ge-Se-Te fibers with the following core diameters 8 and 9 µm. Such fibers still exhibit normal dispersion at the pump wavelength (see Fig. 2, β_2 is in the range 0.15 - 0.18 ps^2 m^{-1}) but their ZDW is now close to 4.0-4.2 µm. Figure 4 shows corresponding experimental (left panels) and numerical (right panels) results obtained for distinct input peak powers. The spectral broadening is again initially driven by self-phase modulation (see low power pumping) until it reaches and overlaps the ZDW for higher input powers. In this case, solitons form beyond 4 µm and experience Raman self-frequency shift towards longer wavelengths. We then obtain SC spectra covering the 2-6µm bandwidth in both SCFs. We also encountered here some damage issues with the 8-µm core SCF at maximum power. However, for all the SC spectra recorded, we are able to confirm such spectral dynamics with numerical simulations. The excellent agreement corroborates the generation of coherent SC spectra over the full bandwidth, even if soliton dynamics occur beyond the 4-µm wave band (only a reduced number of solitons emerge from this nonlinear pulse propagation).

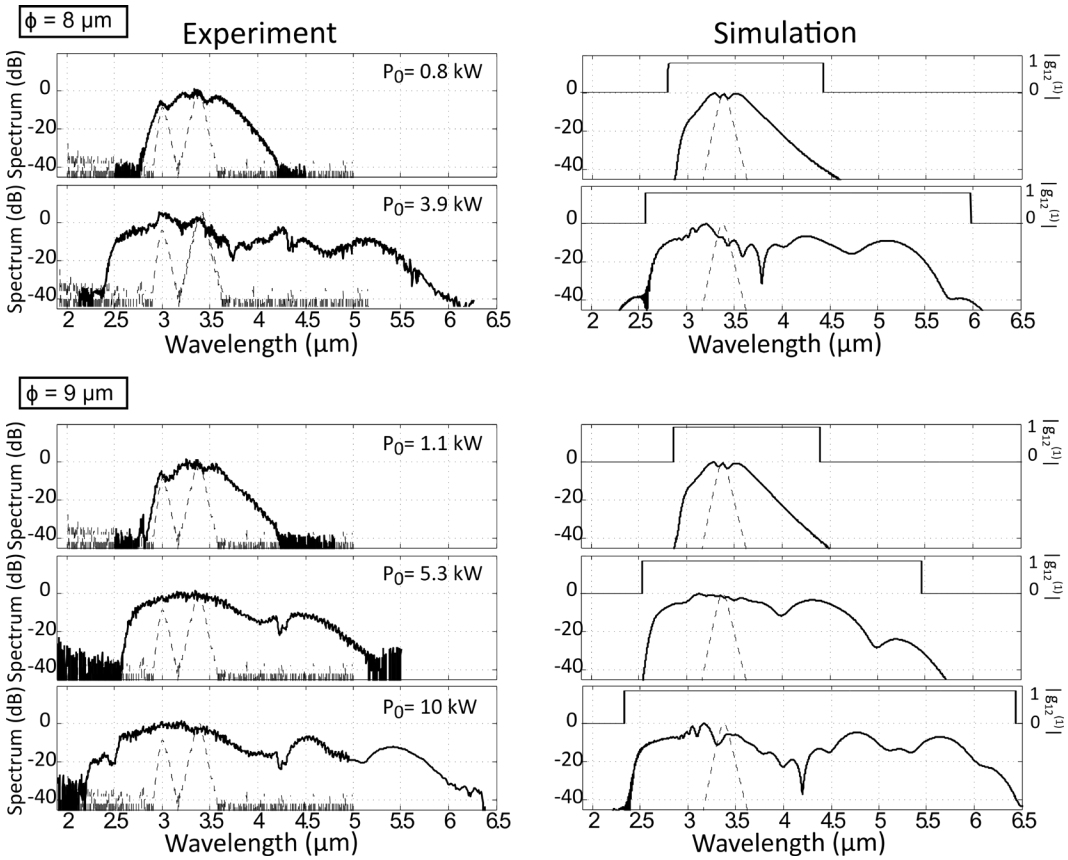

Figure 4. SC spectra obtained in suspended-core Ge-Se-Te fibers with large core diameters (8 and 9 µm) and for distinct input peak powers. Left panels: experimental SC measurements. Dashed lines indicate the spectrum of the input pump source. Right panels: corresponding numerical results of SC generation. Left axis provides the average SC spectrum obtained for 200 simulations. Dashed lines indicate the input pump spectrum considered. Right axis shows the calculated modulus of the complex degree of first-order coherence (a value of 1 denotes perfect coherence).

3.3 SC generation in Ge-Se-Te fibers with small suspended-core

Finally, we investigate SC generation in two suspended-core Ge-Se-Te fibers with smaller core diameters, namely 4 and 5.5 µm. Such fibers now exhibit either anomalous dispersion or nearly null-dispersion at the pump wavelength (see Fig. 2, β_2 is -0.17 and 0.02 ps^2 m^{-1}, respectively) and the ZDW is located at 3.0 or 3.4 µm, respectively. Figure 5 shows corresponding experimental (left panels) and numerical (right panels) results obtained for distinct input peak powers. The spectral broadening is fully driven by soliton dynamics and the formation of phase-matched dispersive waves below the ZDW. Numerical results well confirm again our experiments. Even at low input powers, spectral broadening is very efficient due to low dispersion and high nonlinear coefficient. The closer to the ZDW, the flatter is the resulting SC spectrum (see 5.5-µm core SCF). However, increasing the input peak power significantly degrades the SC coherence since we easily reach input soliton number $N > 10$ for both fibers (higher sensitivity to input noise for such N values). For the 4-µm core SCF, the calculated N value is 14 when $P_0 = 2.5$ kW. Similarly for the 5.5-µm core SCF, the calculated N value is 37 when $P_0 = 3.6$ kW. Moreover, we can note that, for such small core fibers, we were not able to reach the maximum input power due to damage issues of the input fiber facet.

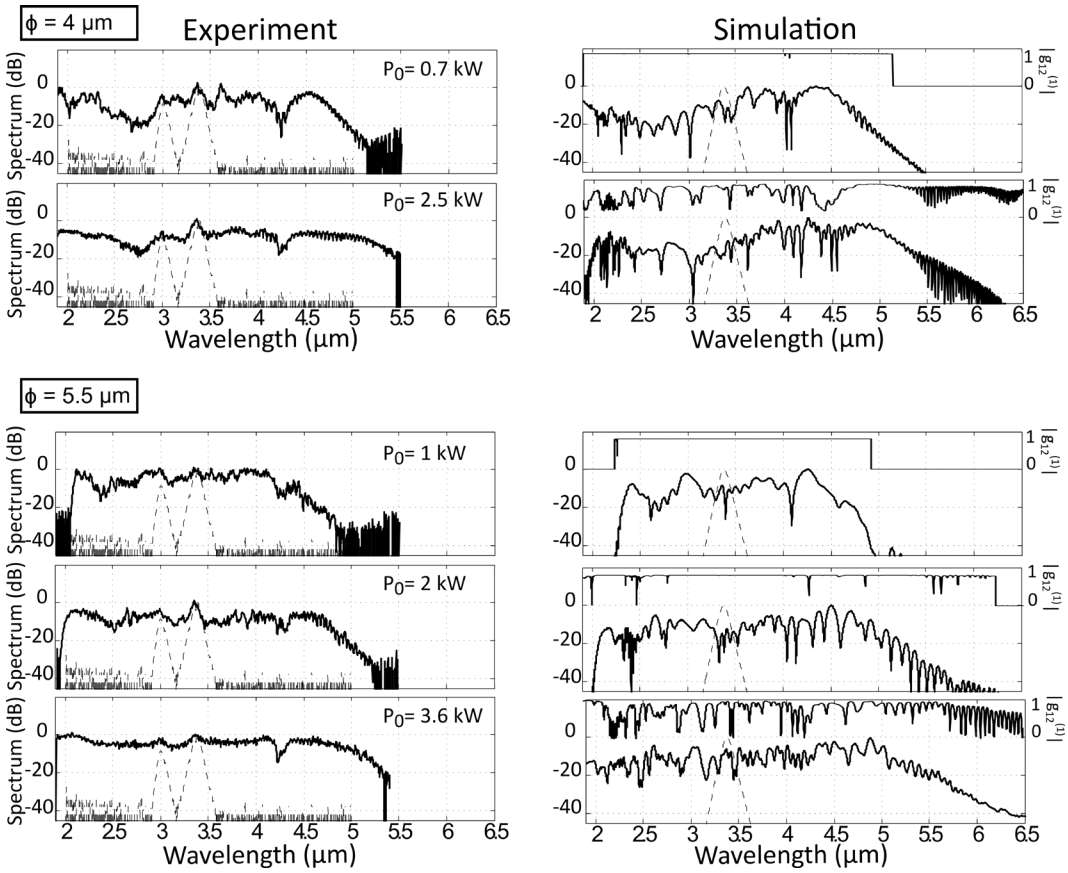

Figure 5. SC spectra obtained in suspended-core Ge-Se-Te fibers with small core diameters (4 and 5.5 μm) and for distinct input peak powers. Left panels: experimental SC measurements. Dashed lines indicate the spectrum of the input pump source. Right panels: corresponding numerical results of SC generation. Left axis provides the average SC spectrum obtained 200 simulations. Dashed lines indicate the input pump spectrum considered. Right axis shows the calculated modulus of the complex degree of first-order coherence (a value of 1 denotes perfect coherence).

4 Discussion

From the above analysis, we can distinguish three configurations, namely, (i) the pumping in the strong normal dispersion regime (i.e., step-index fibers), which rather leads to narrower spectral broadenings and preservation of full coherence, (ii) the pumping in the low normal dispersion close to ZDW that enables efficient spectral broadening with limited soliton dynamics but still preserving coherence (i.e., suspended-core fibers with a large core), and (iii) the common direct pumping at ZDW or in the anomalous dispersion regime with the broadest SC spectra at moderate powers but

coherence degradation (i.e., suspended-core fibers with a small core). These three SC pictures are illustrated in Figs. 6a-6c, where the corresponding SC evolution as a function of propagation distance is depicted for the following fibers: 10-µm core SIF, 8-µm core SCF, and 5.5-µm core SCF. One can retrieve the nonlinear dynamics above described and obtained for the maximal input power we reached in experiments. In Fig. 6d, we plot the corresponding evolution of calculated soliton number N for increasing peak powers, we clearly note the quite different growth of N driven by the fiber dispersions. We can expect to preserve full coherence of the SC spectrum even at higher peak powers still possible (~10-15 kW) for both 10-µm core SIF and 8-µm core SCF.

Unfortunately, we experienced several irreversible damages on most of our fibers as mentioned in previous section. The nature of the damages is mainly thermal accumulation leading to damaged area over the input fiber core with smooth melting features. The composition of chalcogenide glasses is known to impact the laser damage threshold, as well as laser pulse parameters (duration and repetition rate) drive the damaged mechanisms [23-24]. Here, this typical laser-induced melting observed at high repetition rate (i.e., 25 MHz) occurs for different powers as a function of the fiber under test. In particular, we noticed that SIFs were less robust than SCFs when considering the same core size. For instance, we were able to test the 9-µm core SCF up to the maximum power available in contrast to the SIFs even with larger cores. Such a distinct behavior can be explained by the surrounding air holes in the SCF, which helps to the dissipation of detrimental thermal accumulation in the fiber core. The latter was successfully confirmed by few tests at higher powers in some fibers but at a decreased repetition rate, namely by using of rotating optical chopper at 15 kHz to produce trains of femtosecond pulses.

Finally, we investigated numerically the possible SC extension that could be expected without damage with same coupling efficiency as obtained previously. In practice, improved laser damage threshold as well as higher coupling factors for chalcogenide fibers can be obtained through several post-processing techniques such as traditional antireflection coatings, fiber end-caps, or more complex patterning of input surfaces (e.g., the so-called “moth eye” structure) [25]. Figures 6e-6g show the corresponding numerical results of SC generation. In the 10-µm core SIF, we could reach the 6-µm wavelength edge still in the coherent SC regime. Similarly, we could cover the 2-7µm bandwidth with the 8-µm core SCF. On the contrary, incoherent SC extending up to 8 µm will be again obtained in the 5.5-µm core SCF.

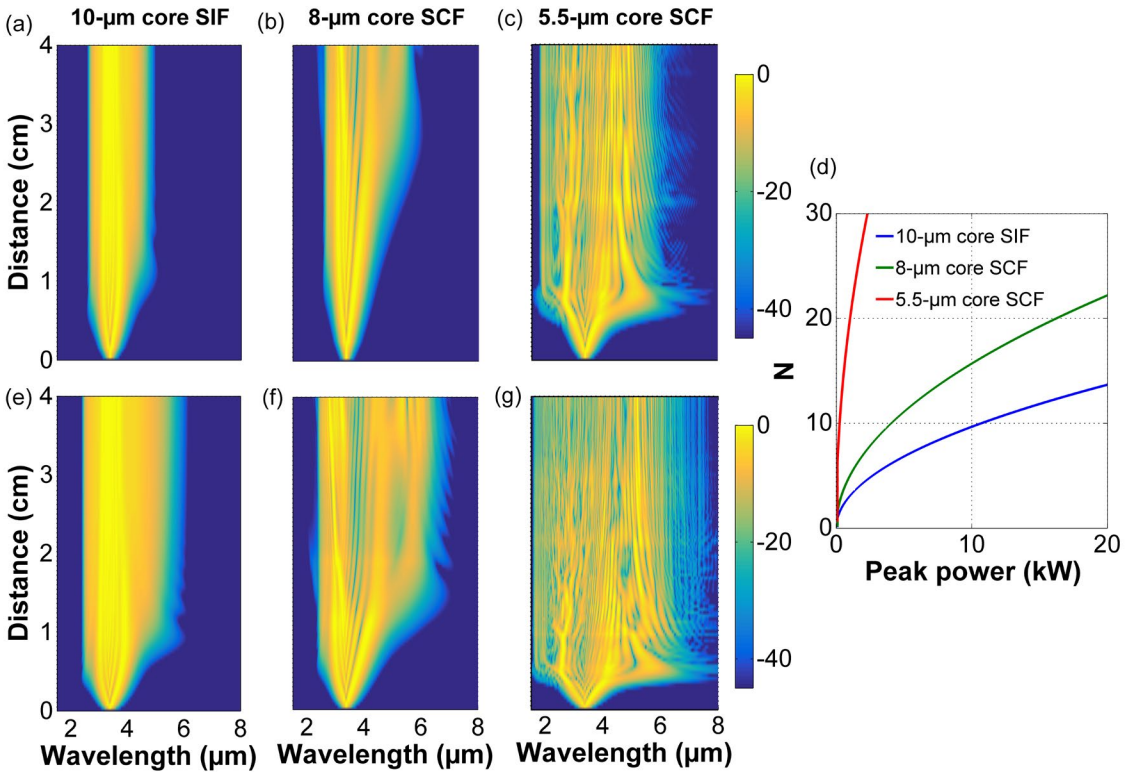

Figure 6. (a-c) Numerical SC evolution as a function of propagation distance for the respective following fibers: 10-μm SIF ($P_0 = 6.7$ kW), 8-μm core SCF ($P_0 = 3.9$ kW), and 5.5-μm core SCF ($P_0 = 3.6$ kW). (d) Calculated soliton number for the same fibers as a function of input peak power. (e-g) Numerical SC evolution as a function of propagation distance for the respective following fibers: 10-μm SIF ($P_0 = 13.7$ kW), 8-μm core SCF ($P_0 = 9$ kW), and 5.5-μm core SCF ($P_0 = 7$ kW).

5 Conclusion

In summary, we studied experimentally and numerically SC generation in various dispersion-engineered Ge-Se-Te fibers pumped by a mid-IR fiber-based soliton source. Our analysis shows that distinct nonlinear pulse propagation regimes can be chosen according to the required tailoring of the supercontinuum source (bandwidth, coherence, flatness). Moreover, we demonstrate that very short segments (cm-long) of our fibers are sufficient to provide the maximal spectral broadening from the mid-IR fiber laser. In particular, we demonstrated coherent SC generation over the 2-6 μm range in a 4 cm-long fiber with up to 50-mW output average power at a repetition rate of 25 MHz. Future developments and improvements of such all-fiber systems capable of tailoring mid-IR SC generation and related coherence properties are an important step towards the

widespread availability of robust and compact SC sources. Within this context, it is worth to mention the very recent work by Tiliouine et al. that demonstrates an all-fiber format source of high-peak power fs pulses above 4 μm by soliton self-frequency shift and its application to mid-IR SC in a chalcogenide fiber [26].

Funding

This work was supported by the French National Research Agency (Project PROTEUS, contract ANR-17-CE08-0042-04; ISITE-BFC program, contract ANR-15-IDEX-03, Projects SCUVIRA & BRIGHT), and the Council of the French Bourgogne Franche-Comté region.

References

[1] T. Sylvestre, E. Genier, A. N. Ghosh, P. Bowen, G. Genty, J. Troles, A. Mussot, A. C. Peacock, M. Klimczak, A. M. Heidt, J. C. Travers, O. Bang, and J. M. Dudley, "Recent advances in supercontinuum generation in specialty optical fibers," J. Opt. Soc. Am. B **38**, F90-F103 (2021).

[2] R. A. Martinez, G. Plant, K. Guo, B. Janiszewski, M. J. Freeman, R. L. Maynard, M. N. Islam, F. L. Terry, O. Alvarez, F. Chenard, R. Bedford, R. Gibson, and A. I. Ifarraguerri, "Mid-infrared supercontinuum generation from 1.6 to >11 μm using concatenated step-index fluoride and chalcogenide fibers," Opt. Lett. **43**, 296-299 (2018).

[3] S. Venck, F. St-Hilaire, L. Brilland, A. N. Ghosh, R. Chahal, C. Caillaud, M. Meneghetti, J. Troles, F. Joulain, S. Cozic, S.Poulain, G. Huss, M. Rochette, J. M. Dudley, and T. Sylvestre, "2–10 μm mid-infrared fiber-based supercontinuum laser source: experiment and simulation," Laser Photon. Rev. **14**, 2000011 (2020).

[4] G. Woyessa, K. Kwarkye, M. K. Dasa, C. R. Petersen, R. Sidharthan, S. Chen, S. Yoo, and O. Bang, "Power stable 1.5–10.5 μm cascaded mid-infrared supercontinuum laser without thulium amplifier," Opt. Lett. **46**, 1129-1132 (2021).

[5] C. R. Petersen, P. M. Moselund, L. Huot, L. Hooper, and O. Bang, "Towards a table-top synchrotron based on supercontinuum generation", Infrared Phys. Technol. **91**, 182-186 (2018).

[6] F. Borondics, M. Jossent, C. Sandt, L. Lavoute, D. Gaponov, A. Hideur, P. Dumas, and S. Février, "Supercontinuum-based Fourier transform infrared spectromicroscopy", Optica **5**, 378-381 (2018).

[7] I. Zorin, P. Gattinger, A. Ebner, and M. Brandstetter, "Advances in mid-infrared spectroscopy enabled by supercontinuum laser sources," Opt. Express **30**, 5222-5254 (2022).

[8] G. Genty, S. Coen, and J. M. Dudley, "Fiber supercontinuum sources," J. Opt. Soc. Am. B **24**, 1771-1785 (2007).

[9] A. Rampur, D.-M. Spangenberg, B. Sierro, P. Hänzi, M. Klimczak, and A. M. Heidt, "Perspective on the next generation of ultra-low noise fiber supercontinuum sources and their emerging applications in spectroscopy, imaging, and ultrafast photonics," Appl. Phys. Lett. **118**, 240504 (2021).

[10] D. D. Hudson, S. Antipov, L. Li, I. Alamgir, T. Hu, M. El Amraoui, Y. Messaddeq, M.Rochette, S. D. Jackson, and A. Fuerbach, "Toward all-fiber supercontinuum spanning the mid-infrared," Optica **4**, 1163-1166 (2017).

[11] L-R. Robichaud, S. Duval, L-P. Pleau, V. Fortin, S. Toubou Bah, S. Châtigny, R. Vallée, and M. Bernier, "High-power supercontinuum generation in the mid-infrared pumped by a soliton self-frequency shifted source", Opt. Express **28**, 107-115 (2020).

[12] R. Salem, Z. Jiang, D. Liu, R. Pafchek, D. Gardner, P. Foy, M. Saad, D. Jenkins, A. Cable, and P. Fendel, "Mid-infrared supercontinuum generation spanning 1.8 octaves using step-index indium fluoride fiber pumped by a femtosecond fiber laser near 2 μm," Opt. Express **23**, 30592-30602 (2015).

[13] B. Kibler, A. Lemière, J.-T. Gomes, D. Gaponov, L. Lavoute, F. Désévédavy, and F. Smektala, "Octave-spanning coherent supercontinuum generation in a step-index tellurite fiber and towards few-cycle pulse compression at 2 μm", Opt. Commun. **488**, 126853 (2021).

[14] S. Duval, M. Bernier, V. Fortin, J. Genest, M. Piché, and R. Vallée, "Femtosecond fiber lasers reach the mid-infrared," Optica **2**, 623-626 (2015).

[15] S. Duval, J.-C. Gauthier, L.-R. Robichaud, P. Paradis, M. Olivier, V. Fortin, M. Bernier, M. Piché, and R. Vallée, "Watt-level fiber-based femtosecond laser source tunable from 2.8 to 3.6 μm," Opt. Lett. **41**, 5294-5297 (2016).

[16] A Lemière, F Désévédavy, P. Mathey, P. Froidevaux, G. Gadret, J.-C. Jules, C. Aquilina, B. Kibler, P. Béjot, F. Billard, O. Faucher, and F. Smektala, "Mid-infrared supercontinuum generation from 2 to 14 μm in arsenic- and antimony-free chalcogenide glass fibers," J. Opt. Soc. Am. B **36**, A183-A192 (2019).

[17] A Lemière, F Désévédavy, B. Kibler, P. Mathey, G. Gadret, J.-C. Jules, C. Aquilina, P. Béjot, F. Billard, O. Faucher, and F. Smektala, "Mid-infrared two-octave spanning supercontinuum generation in a Ge–Se–Te glass suspended core fiber," Las. Phys. Lett. **16**, 075402 (2019).

[18] A Lemière, R. Bizot, F Désévédavy, G. Gadret, J.-C. Jules, P. Mathey, C. Aquilina, P. Béjot, F. Billard, O. Faucher, B. Kibler, and F. Smektala, "1.7–18 μm mid-infrared supercontinuum generation in a dispersion-engineered step-index chalcogenide fiber," Res. Phys. **26**, 104397 (2021).

[19] A. H. Moharram, M. A. Hefni, and A. M. Abdel-Baset, "Short and intermediate range order of $Ge_{20}Se_{80-x}Te_x$ glasses," J. Appl. Phys. **108**, 073505 (2010).

[20] L. Sun, F. Chen, Y. Xu, Y. Huang, S. Liu, Z. Zhao, X. Wang, P. Zhang, S. Dai, and X. Zhang, "Investigation of the third-order nonlinear property of Ge–Se–Te glasses at mid-infrared," Appl. Phys. A **122**, 816 (2016).

[21] A. M. Heidt, J. S. Feehan, J. H. V. Price, T. Feurer, "Limits of coherent supercontinuum generation in normal dispersion fibers," J. Opt. Soc. Amer. B **34**, 764-775 (2017).

[22] C. Finot, B. Kibler, L. Provost, S. Wabnitz, "Beneficial impact of wave-breaking for coherent continuum formation in normally dispersive nonlinear fibers", J. Opt. Soc. Amer. B **25**, 1938-1948 (2008).

[23] C. You, S. Dai, P. Zhang, Y. Xu, Y. Wang, D. Xu, and R. Wang, "Mid-infrared femtosecond laser-induced damages in As2S3 and As_2Se_3 chalcogenide glasses," Sci. Rep. **7**, 6497 (2017).

[24] M. Zhang, T. Li, Y. Yang, H. Tao, X. Zhang, X. Yuan, and Z. Yang, "Femtosecond laser induced damage on Ge-As-S chalcogenide glasses," Opt. Mater. Express **9**, 555-561 (2019).

[25] V. Fortin, Y. Ozan Aydin, M. Bernier, R. Vallée, M. Rochette, F. Chenard, O. Alvarez, L. E. Busse, L. B. Shaw, R. R. Gattass, and J. S. Sanghera, "Chapter 5 - Post-processing soft glass optical fibers," Eds: S. Jackson, M. Bernier, R. Vallée, In Woodhead Publishing Series in Electronic and Optical Materials, Mid-Infrared Fiber Photonics, Woodhead Publishing, 2022, Pages 233-302.

[26] I. Tiliouine, G. Granger, Y. Leventoux, C. E. Jimenez, J. Melek, V. Couderc, and S. Février, "Two-octave mid-infrared supercontinuum pumped by a 4.5 μm femtosecond fiber source," in Conference on Lasers and Electro-Optics, Technical Digest Series (Optica Publishing Group, 2022), paper JM3E.5.